Available online at www.sciencedirect.com
SCIENCE DIRECT®
PERGAMON
International Journal of Heat and Mass Transfer 46 (2003) 2253–2261
International Journal of HEAT and MASS TRANSFER
www.elsevier.com/locate/ijhmt

Numerical simulation of developing natural convection in an enclosure due to rapid heating

Murat K. Aktas, Bakhtier Farouk *

Department of Mechanical Engineering and Mechanics, Drexel University, 3141 Chestnut Street, Philadelphia, PA 19104, USA

Received 17 December 2001; received in revised form 18 September 2002

Abstract

Effects of thermoacoustic wave motion on the developing natural convection process in a compressible gas-filled square enclosure were investigated numerically. In the cases considered, the left wall temperature is raised rapidly (impulsively or gradually) while the right wall is held at a specified temperature. The top and the bottom walls of the enclosure considered are thermally insulated. The numerical solutions of the full Navier–Stokes equations were obtained by employing a highly accurate flux-corrected transport algorithm for the convection terms and by a central differencing scheme for the viscous and diffusive terms. The strength of the pressure waves associated with the thermoacoustic effect and resulting flow patterns are found to be strongly correlated to the rapidity of the wall heating process. Fluid thermal diffusivity was found to affect the strength of the thermoacoustic waves and the resulting interaction with the buoyancy-induced flow.

Keywords: Thermoacoustic wave; Natural convection

1. Introduction

When a compressible fluid is subjected to a rapid temperature increase at a solid wall, part of the fluid in the immediate vicinity of the boundary expands. This gives rise to a fast increase in the local pressure, and leads to the production of pressure waves called thermoacoustic waves. The heat transfer effects of such waves may be very significant when the fluid is close to the thermodynamic critical point or when other modes of convection are weak or absent. This motion may cause unwanted disturbances in otherwise static processes like cryogenic storage or may introduce a convective heat transfer mode to the systems in zero-gravity environment where it is assumed that conduction is the only heat transfer mode. Low-heat-diffusivity character of near-critical conditions makes thermoacoustic convection mode of heat transport very significant for cryogenic storage systems which involve rather weak diffusive and convective transport of heat especially in reduced gravity environment. Because of high density and compressibility values of fluids in these systems, strong thermoacoustic waves are produced and heat transfer effects of these waves become critical due to the possibility of sudden phase change in the storage system.

The problem of thermoacoustic waves in a quiescent semi-infinite body of a perfect gas, subjected to a step change in temperature at the solid wall was studied analytically [1] in order to determine how the sound intensity depends on the wall temperature history. The one-dimensional compressible flow equations were linearized and a closed-form asymptotic solution was obtained using a Laplace transform technique. A simplified model (the hyperbolic equation of conduction) for thermoacoustic motion was compared with one-dimensional Navier–Stokes equations model of the phenomena and limitations of the simplified approach was discussed [2]. A more general class of solutions for the thermoacoustic waves was obtained by using the Laplace transform method with numerical inversion for equations of the linear wave model for step and gradual

* Corresponding author. Tel.: +1-215-895-2287; fax: +1-215-895-1478.
E-mail address: bfarouk@cbis.ece.drexel.edu (B. Farouk).

0017-9310/03/$ - see front matter
doi:10.1016/S0017-9310(02)00522-7

Nomenclature

A	overheat ratio
E	total energy
g	gravitational acceleration
k	thermal conductivity
L	width and height of the enclosure
Nu	Nusselt number ($= hL/k_f^*$)
p	pressure
Pr	Prandtl number ($= v_f^*/\alpha_f^*$)
q	heat flux
R	specific gas constant
Ra	Rayleigh number ($= g\beta_f(T_L^* - T_R^*)L^3/v_f^*\alpha_f^*$)
t	time
T	temperature
u	velocity in the horizontal direction
v	velocity in the vertical direction
x	horizontal coordinate
y	vertical coordinate

Greek symbols

α	thermal diffusivity
β	volumetric thermal expansion coefficient ($= 1/T_f^*$)
γ	ratio of specific heats
μ	dynamic viscosity
v	kinematic viscosity
ρ	density
τ	shear stress
τ_c	travel time for the acoustic wave to traverse the enclosure width
τ_h	time constant for wall heating

Superscript

$*$	dimensional variable

Subscripts

0	initial
f	property value evaluated at reference temperature
L	left
M	wall location
n	direction normal to the wall
R	right

changes in the boundary temperature [3]. The equations of the nonlinear wave model were numerically solved using finite differences scheme modified with a Galerkin finite element interpolation in space. A similar analysis for thermoacoustic waves in a confined medium was repeated more recently [4]. In both geometries the medium considered was a gas with Prandtl number of 0.75. Thermoacoustic convection phenomena were experimentally investigated in a cylinder containing air with temperature measurements in normal and reduced gravity environment [5]. No pressure measurement was reported. Experimental measurements of pressure waves generated by rapid heating of a surface were reported in a relatively recent paper [6].

Numerical studies of one- and two-dimensional thermoacoustic waves in a confined region have been carried out [7,8]. These computational studies described finite-difference solutions of the compressible Navier–Stokes equations for a gas with temperature-independent thermophysical properties. The solutions were obtained by employing first-order upwind schemes to solve the governing equations, and as a consequence, the results showed effects of substantial numerical diffusion. The mechanisms of heat and mass transport in a side-heated square cavity filled with a near-critical fluid were explored [9], with special emphasis on the interplay between buoyancy-driven convection and the piston effect. In a recent paper, it was shown that rapid heating of a solid surface bounding a region of gas generates a slightly supersonic wave with positive amplitude in pressure, temperature, density and mass velocity [10]. The one-dimensional predictions were in good qualitative agreement with prior experimental measurements of the shape, amplitude and rate of decay of the pressure waves. Using a high-order numerical scheme, the early time behavior of thermoacoustic waves in a compressible-fluid filled cavity was predicted with a computa-

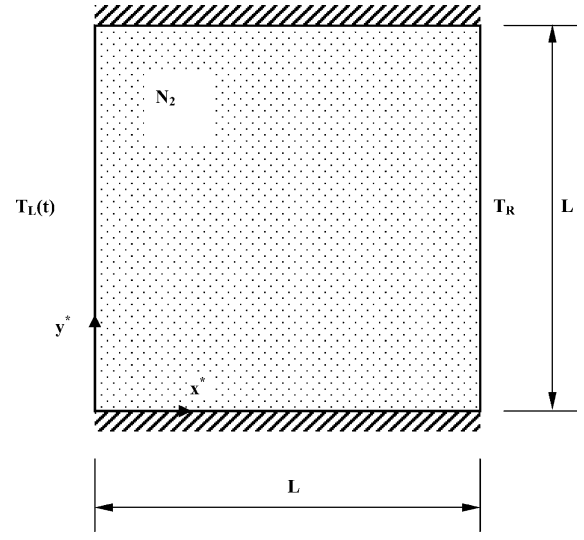

Fig. 1. Geometry and the boundary conditions of the problem.

tional study [11] in which temperature dependent fluid properties were used.

In the present paper, the effects of thermoacoustic waves on buoyancy-induced flow fields are studied for a square enclosure with side length $L = 13$ mm (Fig. 1). The horizontal walls of the square enclosure are considered to be insulated whereas the vertical walls are isothermal. Initially the gas and all walls are in thermal equilibrium ($T^* = T_R^*$ everywhere). At $t^* > 0$, the left wall temperature is increased to a value T_L^* ($T_L^* > T_R^*$) either suddenly or gradually. The strength of the thermoacoustic waves depend on the rapidity of the wall heating, and the interaction effects are significant only for the early times. We also investigate the effects of fluid properties on the interaction process.

2. Mathematical model

Interaction of thermoacoustic waves and buoyancy problem is described by the Navier–Stokes equations for a compressible fluid. These equations is expressed in vector form with dimensionless variables as

$$\frac{\partial \mathbf{U}}{\partial t}+\frac{\partial \mathbf{F}}{\partial x}+\frac{\partial \mathbf{G}}{\partial y}=\frac{\partial \mathbf{F_v}}{\partial x}+\frac{\partial \mathbf{G_v}}{\partial y}+\mathbf{B} \tag{1}$$

where t is the time and x and y refers to the Cartesian coordinates. The vectors represent

$$\mathbf{U}=\begin{bmatrix}\rho\\ \rho u\\ \rho v\\ E\end{bmatrix},\quad \mathbf{F}=\begin{bmatrix}\rho u\\ \rho u^2\\ \rho uv\\ (E+p)u\end{bmatrix},\quad \mathbf{G}=\begin{bmatrix}\rho v\\ \rho uv\\ \rho v^2\\ (E+p)v\end{bmatrix} \tag{2}$$

$$\mathbf{F_v}=\begin{bmatrix}0\\ Pr(\tau_{xx}-p)\\ Pr\tau_{xy}\\ u\tau_{xx}+v\tau_{xy}-\delta q_x\end{bmatrix},\quad \mathbf{G_v}=\begin{bmatrix}0\\ Pr\tau_{xy}\\ Pr(\tau_{yy}-p)\\ u\tau_{xy}+v\tau_{yy}-\delta q_y\end{bmatrix},\quad \mathbf{B}=\begin{bmatrix}0\\ 0\\ \rho RaPr/2\varepsilon\\ \rho vRa/2\varepsilon\end{bmatrix} \tag{3}$$

where ρ is the density, u and v are the velocity components, p is the pressure, g is the gravitational acceleration, Ra is the Rayleigh number, Pr is the Prandtl number and E is the total energy. The components of the stress tensor τ are

$$\begin{aligned}\tau_{xx}&=\mu\left(2\frac{\partial u}{\partial x}-\frac{2}{3}\nabla\cdot\mathbf{v}\right)\\ \tau_{yy}&=\mu\left(2\frac{\partial v}{\partial y}-\frac{2}{3}\nabla\cdot\mathbf{v}\right)\\ \tau_{xy}&=\mu\left(\frac{\partial u}{\partial y}+\frac{\partial v}{\partial x}\right)\end{aligned} \tag{4}$$

where μ is the dynamic viscosity and $\nabla\cdot\mathbf{v}$ is the divergence of the velocity vector. The components of the heat-flux vector are written as

$$q_x=-k\frac{\partial T}{\partial x},\quad q_x=-k\frac{\partial T}{\partial y} \tag{5}$$

where k is the thermal conductivity. The dimensionless variables are

$$\begin{aligned}&x=\frac{x^*}{L},\quad y=\frac{y^*}{L},\quad t=\frac{t^*\alpha_f^*}{L^2}\\ &u=\frac{u^*}{\alpha_f^*/L},\quad v=\frac{v^*}{\alpha_f^*/L}\\ &\rho=\frac{\rho^*}{\rho_f^*},\quad \mu=\frac{\mu^*}{\mu_f^*},\quad \alpha=\frac{\alpha^*}{\alpha_f^*}\\ &k=\frac{k^*}{k_f^*},\quad T=\frac{T^*-T_R^*}{T_L^*-T_R^*}\\ &\varepsilon=\frac{T_L^*-T_R^*}{T_L^*+T_R^*},\quad \delta=\frac{k_f^*L^2(T_L^*-T_R^*)}{\rho_f^*v_f^*\alpha_f^{*2}}\\ &p=\frac{p^*}{\rho_f^*v_f^*\alpha_f^*/L^2},\quad E=\frac{E^*}{\rho_f^*v_f^*\alpha_f^*/L^2}\end{aligned} \tag{6}$$

Rayleigh, Prandtl and Nusselt numbers are defined based on the fluid thermophysical properties evaluated at the reference temperature T_f^*:

$$T_f^*=\frac{T_L^*+T_R^*}{2} \tag{7}$$

Total energy is given by

$$E^*=\frac{\rho^*RT^*}{\gamma-1}+\frac{1}{2}\rho^*(u^{*2}+v^{*2}) \tag{8}$$

Here R is the specific gas constant of the medium and γ is the ratio of specific heats. The temperature is related to the density and pressure through the ideal-gas law:

$$p^*=\rho^*RT^* \tag{9}$$

3. Numerical scheme

The governing equations (except for the diffusion terms) are discretized using a control-volume-based finite-volume method based on the flux-corrected transport (FCT) algorithm. FCT is a high-order, nonlinear,

monotone, conservative and positivity-preserving scheme designed to solve a general one-dimensional continuity equation with appropriate source terms. This scheme has fourth-order phase accuracy and is able to resolve steep gradients with minimum numerical diffusion. In this algorithm, when a flow variable such as a density is initially positive, it remains positive during the computations and no new minimum or maximum values are introduced due to numerical errors in the calculation process. To ensure positivity and stability, a minimum amount of numerical diffusion over the stability limit is added at each time step. Time-step splitting technique is used to solve the two-dimensional problem addressed here. Further details of the FCT algorithm used here are documented in [12]. The diffusion terms (the viscous term in the momentum equations and the conduction terms in the energy equation) were discretized using the central-difference approach and the time-step splitting technique was used to include the terms in the numerical scheme. Time-step splitting technique was also used to include the gravity term in the y-momentum equation and the viscous dissipation terms in the energy equation.

No-slip boundary conditions were used for all the solid walls. Time-dependent boundary conditions for the vertical walls and zero-gradient temperature boundary conditions for the horizontal walls were used. A high-order non-dissipative algorithm such as FCT requires rigorous formulation of the boundary conditions. Otherwise, numerical solutions may show spurious wave reflections at the regions close to boundaries and non-physical oscillations arising from instabilities. In the present computational method, the treatment proposed by Poinsot and Lele [13] was followed for implementing the boundary conditions for the density. Along any solid wall, the density is calculated from

$$\left(\frac{\partial \rho^*}{\partial t^*}\right)_{\mathrm{M}} + \frac{1}{c_{\mathrm{M}}}\left(\frac{\partial p^*}{\partial n} + \rho^* c \frac{\partial u_{\mathrm{n}}^*}{\partial n}\right)_{\mathrm{M}} = 0 \tag{10}$$

where c_{M} is the acoustic speed, M indicates the location of the wall and n is the direction normal to the wall.

4. Results and discussion

Numerical simulations of the thermoacoustic wave motion and its interactions with the buoyancy-induced flow fields were performed for a square enclosure filled with nitrogen gas, initially quiescent at 1 atm pressure and 300 K temperature. For all computations, non-uniform grid structure was employed with 141×141 computational cells. Variation of the fluid properties with temperature was taken into account. Results of our prior investigation [11] on the very short time behavior of the thermoacoustic waves generated by impulsive and gradual heating of a wall were in very good agreement with the results given in the literature. In the present study, longer time behavior of the pressure waves produced by a step change (impulsive heating) at the left wall temperature of the enclosure was investigated. For impulsive heating, the left wall temperature is given by

$$T_{\mathrm{L}}^* = \begin{cases} T_0^*, & t^* = 0 \\ T_0^*(A+1), & t^* > 0 \end{cases} \tag{11}$$

where T_0^* is the initial temperature ($T_0^* = T_{\mathrm{R}}^*$) and A is the overheat ratio,

$$A = \frac{T_{\mathrm{L}}^* - T_{\mathrm{R}}^*}{T_{\mathrm{R}}^*} \tag{12}$$

In a numerical scheme, 'impulsive heating' can be approximated by the value of the first time step. In the present computations the first time step is rather small, 1.04×10^{-7} s. Results are shown in Fig. 2 for the midpoint pressure of the enclosure, where the Rayleigh number is 10^4. For the two overheat ratios considered ($A = 1/3$ and 1) the pressure increases continuously, however, the presence of thermoacoustic waves is evident. The pressure value shows a distinctive peak whenever the thermoacoustic wave crosses the midpoint. Strength of the pressure wave is strongly correlated to the overheat ratio and pressure oscillations are damped with increasing time. The effect of the gravitational acceleration was found negligible at the early stages of the flow development and thermoacoustic behavior.

In practice, due to the thermal inertia of a wall and a heating system and unavoidable heat losses to the environment, it is difficult to generate a step change (impulsive heating) in the wall temperature. Therefore, the effect of the rapidity of the wall heating process (gradual heating) on the thermoacoustic wave behavior was investigated and results are shown in Fig. 3 ($A = 1/3$ and $Ra = 10^4$) for the time variation of the midpoint pressure for three different heating conditions. The gradual heating process was considered with an exponential expression:

$$T_{\mathrm{L}}^*(t^*) = T_0^*[1 + A(1 - \mathrm{e}^{-t^*/\tau_{\mathrm{h}}})] \tag{13}$$

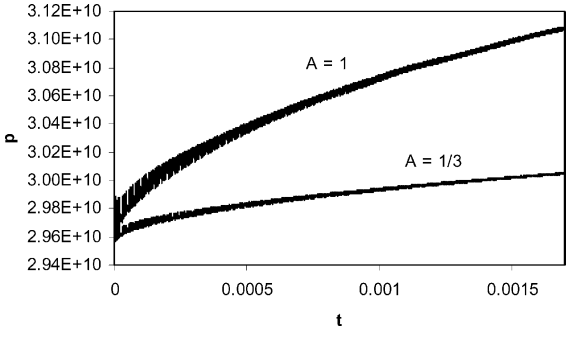

Fig. 2. Variation of pressure with time at the midpoint of the enclosure for two different overheat ratio ($Ra = 10^4$).

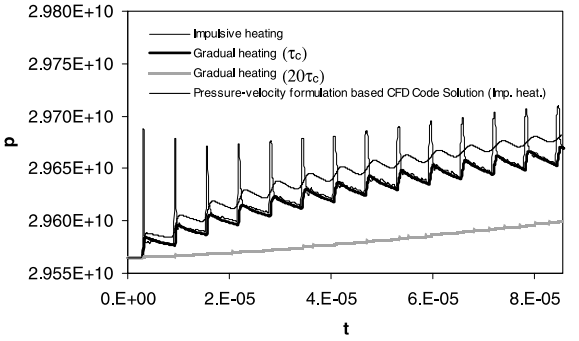

Fig. 3. Effect of the rapidity of the left wall heating process on the midpoint pressure of the enclosure ($\tau_c = 36.82 \times 10^{-6}$ s, $A = 1/3$, $Ra = 10^4$).

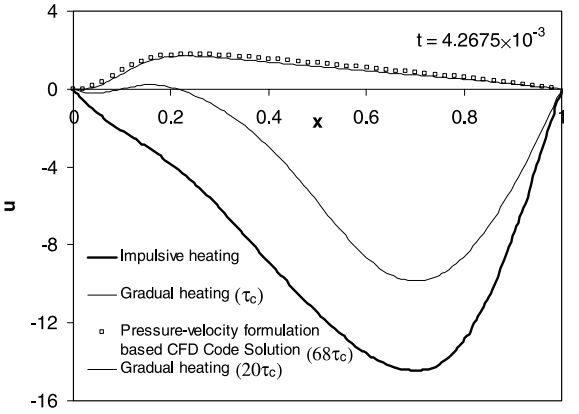

Fig. 4. Variation of the x-component of the velocity vector along the horizontal mid-plane of the enclosure ($Ra = 10^4$).

where τ_h is the time constant of the wall heating process. For impulsive heating, ideally $\tau_h = 0$. For the two gradual heating cases given in Fig. 3, τ_h was τ_c and $20\tau_c$, respectively, where τ_c is the travel time of sound waves for the length of the enclosure ($\tau_c = 36.82 \times 10^{-6}$ s). Fig. 3 indicates that the rapidity of the wall heating process has very significant effect on the strength of the pressure waves. When $\tau_h = 20\tau_c$, the strength of the thermoacoustic waves are negligible. Fig. 3 also shows the results of a pressure–velocity formulation based Navier–Stokes code solution for the impulsive heating case. Pressure–velocity formulation based Navier–Stokes code we used is based on discretisation of governing equation with finite-volume technique and employs implicit time integration scheme. In this method, pressure is updated during the solution process from momentum equation and velocity components are corrected to satisfy continuity equation. The grid structure and time step size are identical for the density–velocity formulation of the Navier–Stokes equations employing the FCT algorithm and the pressure–velocity formulation of the Navier–Stokes code. We find that when sufficiently small time steps are used (time steps that satisfies the Courant condition), the pressure–velocity formulation of the Navier–Stokes code predict the propagation of the thermoacoustic waves. However, a comparison between the results clearly indicates that pressure–velocity formulation based Navier–Stokes code is not able to predict the amplitude of pressure waves accurately.

Computations were then carried out for longer times (up to $t^* = 0.025$ s) at which the buoyancy-induced flow fields develop. This value is very large compared to the acoustic time scale ($t^* = 36.82 \times 10^{-6}$ s) and is comparable to the value of the viscous ($t^* = 0.1$ s) and thermal ($t^* = 0.058$ s) time scales which are growth times of the viscous and thermal boundary layers [14] for the natural convection problem considered. In Fig. 4, results obtained for the x-component of the velocity vector are shown along the horizontal mid-plane of the enclosure for $A = 1/3$ and $Ra = 10^4$ at $t^* = 0.025$ s ($t = 4.2675 \times 10^{-3}$). These velocity profiles show the significance of the thermoacoustic motion on transient heat convection process. In case of impulsive heating, strong pressure waves completely change the flow characteristics in the enclosure and thermoacoustic wave effect dominates the fluid motion. This effect is very clearly seen on the negative values of the u velocity in Fig. 4. With gradual heating (where $\tau_h = \tau_c$) thermoacoustic effect loses its power and expected flow characteristics of the buoyancy-driven fluid motion is observed (gradual heating, $\tau_h = 20\tau_c$). In Fig. 4, we also show the results from the pressure–velocity formulation of the Navier–Stokes code for a gradual heating case ($\tau_h \cong 68\tau_c$). Since the heating process is slow, no thermoacoustic waves are generated.

Fig. 5a–d shows the velocity vectors for the case where $A = 1/3$ and $Ra = 10^4$. All four figures show the velocity field in the enclosure at a given time ($t^* = 0.025$ s, $t = 4.2675 \times 10^{-3}$), with different heating conditions of the left wall. For impulsive heating (Fig. 5a) very strong back flow is observed as a result of the pressure wave reflection on the right wall. This behavior significantly changes in case of gradual heating ($\tau_h = \tau_c$, Fig. 5b; $\tau_h = 5\tau_c$, Fig. 5c; $\tau_h = 20\tau_c$, Fig. 5d). It is interesting to note that though the characteristic time for acoustic wave propagation in the enclosure ($\tau_c = 36.82 \times 10^{-6}$ s) is rather small, the effects of the thermoacoustic waves are significant even at $t^* = 0.025$ s, as shown in Fig. 5a for impulsive heating.

Corresponding pressure and temperature fields (at $t^* = 0.025$ s, $t = 4.2675 \times 10^{-3}$) for impulsive heating (as shown in Fig. 5a) case are given in Fig. 6a,b; and for gradual heating case ($\tau_h = 5\tau_c$, as shown in Fig. 5c) are given in Fig. 7a,b. In case of impulsive heating (Fig. 6a) pressure in the enclosure is relatively high and does not vary in the vertical direction. Comparing Fig. 5a with

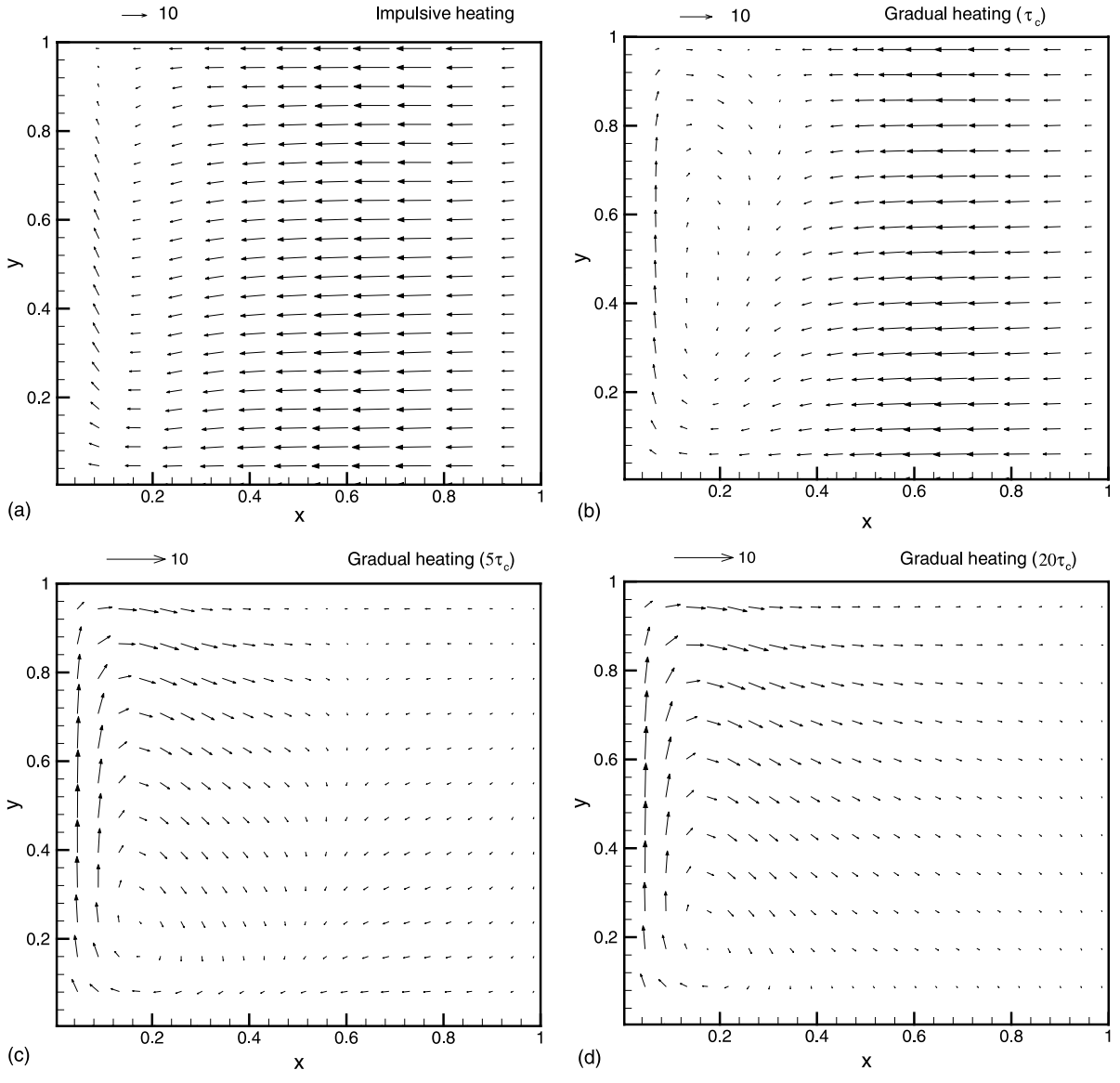

Fig. 5. Variation of the velocity vectors and flow field depending on the rapidity of the wall heating process at $Ra = 10^4$, $t = 4.2675 \times 10^{-3}$ ($t^* = 0.025$ s): (a) impulsive heating; (b) gradual heating (τ_c); (c) gradual heating ($5\tau_c$); (d) gradual heating ($20\tau_c$).

Fig. 6a, it is seen that the location of the thermoacoustic wave front is characterized by the location ($x \cong 0.6$) of the highest velocity, as well as the highest pressure. In this region, temperature gradient in horizontal direction is very low (Fig. 6b). For the gradual heating case considered in Fig. 5c, no thermoacoustic wave front is found as the buoyancy-induced flow field can develop unimpeded. Consequently, the pressure field shown in Fig. 7a is fairly uniform. Comparing Fig. 5c with Fig. 7b, it is seen that in the region where there is no horizontal fluid motion ($x \cong 0.6$) the heat transport is very low.

Traditional computational fluid dynamics techniques employing pressure–velocity formulation of the Navier–Stokes equations fail to predict the thermoacoustic effect on the transient buoyancy-driven motion for rapid heating. In earlier studies [7,8], the signature of the thermoacoustic waves were not reported accurately—perhaps due to significant numerical diffusion and the lack of 'characteristic (wave)' type wall boundary conditions in the scheme [13]. The flow fields given in the earlier papers also do not clearly demonstrate the effects of thermoacoustic waves on the buoyancy-induced flows.

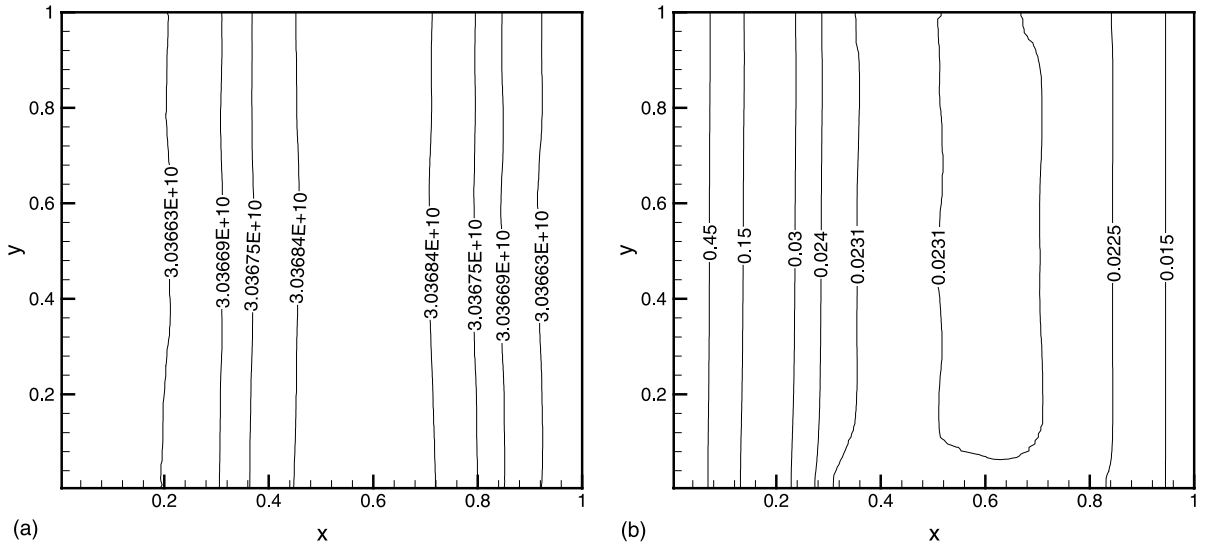

Fig. 6. Variation of pressure and temperature in the enclosure at $t = 4.2675 \times 10^{-3}$ ($t^* = 0.025$ s): impulsive heating ($Ra = 10^4$).

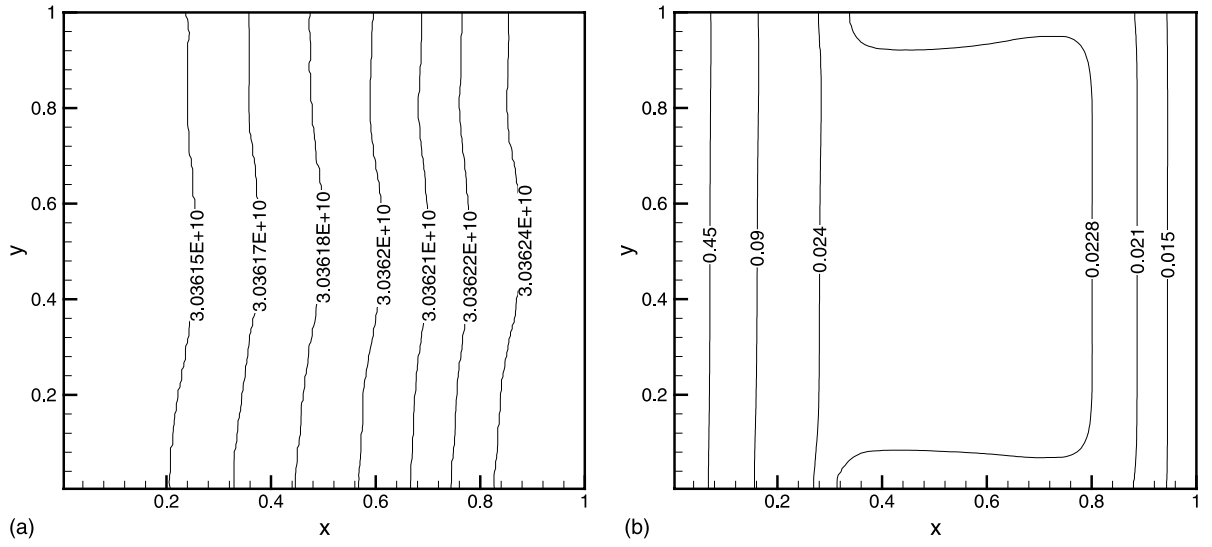

Fig. 7. Variation of pressure and temperature in the enclosure at $t = 4.2675 \times 10^{-3}$ ($t^* = 0.025$ s): gradual heating ($5\tau_c$, $Ra = 10^4$).

The effect of fluid properties on the thermoacoustic phenomena was investigated next by considering a helium filled enclosure. Helium has approximately nine times larger thermal diffusivity than nitrogen. With the same overheat ratio ($A = 1/3$) and the same temperature difference ($T_L^* - T_R^*$), thermoacoustic waves generated by sudden (impulsive) heating of the left wall of the enclosure travel faster (1016 m/s) and generate stronger pressure waves in helium (Fig. 8a) compared to the waves generated in nitrogen. The stronger thermoacoustic waves in helium are due to the small value of the density of helium. In Fig. 8b, the time variation of the Nusselt number at the right wall is shown for the helium and the nitrogen cases for impulsive heating. Higher heat transfer rates are achieved for helium at the right wall of the enclosure at the instances when the acoustic waves impinge on the wall. The higher values in the heat transfer coefficient are due to the stronger thermoacoustic waves produced in helium. Due to the faster acoustic speed of helium, the peaks (caused by wall impingement) occur more frequently than that for nitrogen.

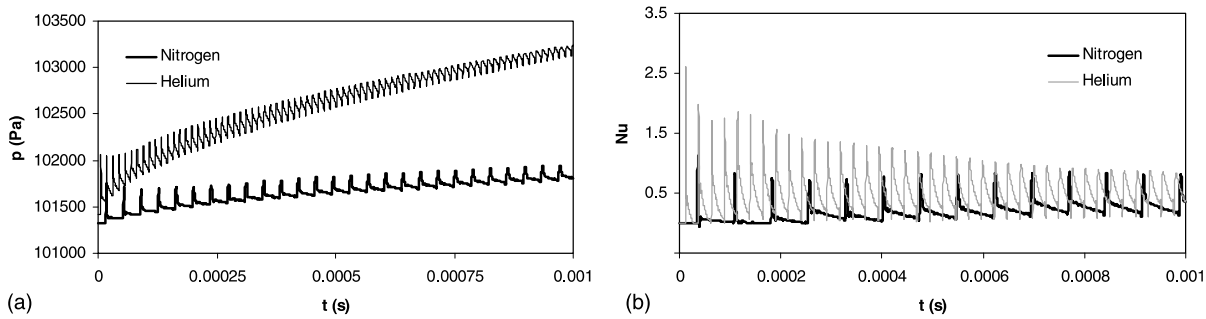

Fig. 8. Effect of thermoacoustic wave motion on (a) midpoint pressure and (b) Nusselt number at the right wall of the enclosure for two different gases.

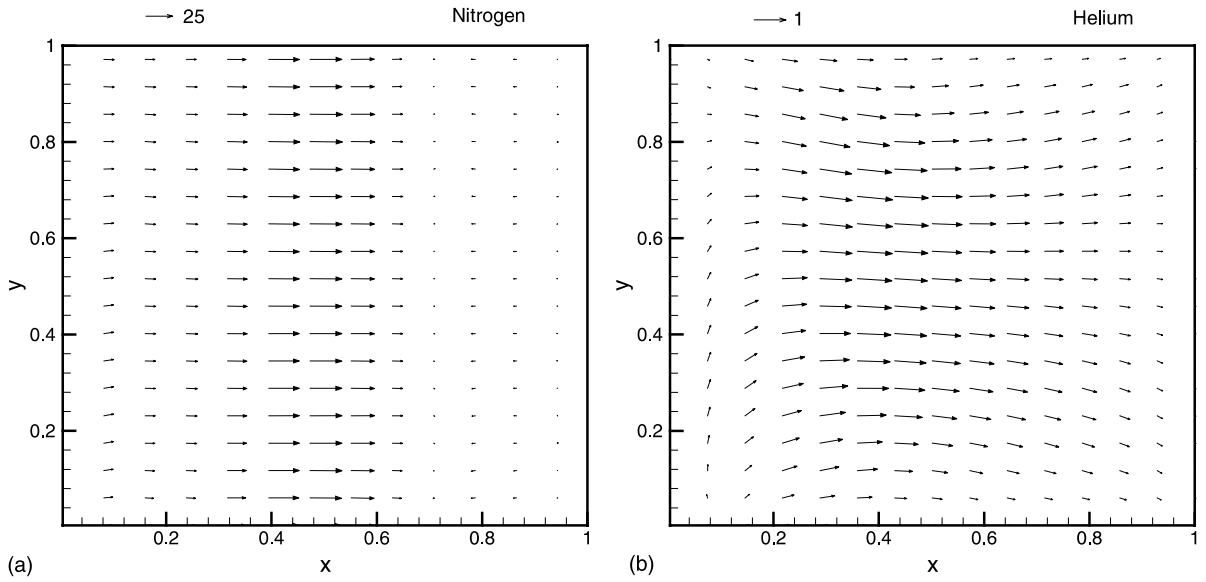

Fig. 9. Distribution of the velocity vectors in the flow field for two different gases at $t^* = 0.01$ s: (a) nitrogen; (b) helium.

For the same heating condition, computations were also carried out for longer time to investigate the development of the flow field for the helium case. Instantaneous velocity vectors are shown in Fig. 9a,b for nitrogen and helium at $t^* = 0.01$ s, respectively due to impulsive heating. For both cases, the temperature difference $(T_L^* - T_R^*)$ and geometry are the same. In nitrogen (Fig. 9a), thermoacoustic waves and resulting flow are relatively strong and the flow field appears to be one-dimensional. However, in helium due to the high thermal diffusivity and the higher frequency of wall reflection, the thermoacoustic waves (though stronger at the time of inception) decay faster. Hence, in Fig. 9b, the flow field for helium at $t^* = 0.01$ s appears to be buoyancy dominated and the effects of thermoacoustic waves are less dominant.

5. Conclusions

The effects of the thermoacoustic phenomena on the transient natural convection process in an enclosure were studied by solving the unsteady compressible Navier–Stokes equations. The effects of the pressure (thermoacoustic) waves on the transient natural heat convection process and flow development were determined by utilizing a highly accurate FCT algorithm. Thermoacoustic waves were generated by increasing the left wall temperature of the enclosure impulsively (suddenly) or gradually and rapidity of the wall heating process was observed to be the leading parameter on the strength of the thermoacoustic waves. Also, the strength of the pressure waves was found directly proportional to the temperature increase ratio on the wall. Significant

effect of the fluid thermal diffusivity on thermoacoustic convection phenomena was observed while the effect of the gravitational acceleration was found negligible on thermoacoustic behavior for early times.

References

[1] L. Trilling, On thermally induced sound fields, J. Acoustical Soc. Am. 27 (1955) 425–431.
[2] S.W. Churchill, M.A. Brown, Thermoacoustic convection and the hyperbolic equation of conduction, Int. Commun. Heat Mass Transfer 14 (1987) 647–655.
[3] Y. Huang, H.H. Bau, Thermoacoustic waves in a semi-infinite medium, Int. J. Heat Mass Transfer 38 (1995) 1329–1345.
[4] Y. Huang, H.H. Bau, Thermoacoustic waves in a confined medium, Int. J. Heat Mass Transfer 40 (1997) 407–419.
[5] M. Parang, A. Salah-Eddine, Thermoacoustic convection heat-transfer phenomenon, AIAA J. 22 (1984) 1020–1022.
[6] M.A. Brown, S.W. Churchill, Experimental measurements of pressure waves generated by impulsive heating of a surface, AIChE J. 41 (1995) 205–213.
[7] H. Ozoe, N. Sato, S.W. Churchill, The effect of various parameters on thermoacoustic convection, Chem. Eng. Commun. 5 (1980) 203–221.
[8] H. Ozoe, N. Sato, S.W. Churchill, Numerical analyses of two and three dimensional thermoacoustic convection generated by a transient step in the temperature of one wall, Numer. Heat Transfer, Part A 18 (1990) 1–15.
[9] B. Zappoli, S. Amiroudine, P. Carles, J. Ouazzani, Thermoacoustic and buoyancy-driven transport in a square side-heated cavity filled with a near-critical fluid, J. Fluid Mech. 316 (1996) 53–72.
[10] M.A. Brown, S.W. Churchill, Finite-difference computation of the wave motion generated in a gas by a rapid increase in the bounding temperature, Comput. Chem. Eng. 23 (1999) 357–376.
[11] B. Farouk, E.S. Oran, T. Fusegi, Numerical study of thermoacoustic waves in an enclosure, Phys. Fluids 12 (2000) 1052–1061.
[12] J.P. Boris, A.M. Landsberg, E.S. Oran, J.H. Gardner, LCPFCT—A flux-corrected transport algorithm for solving generalized continuity equations, Naval Research Laboratory, Washington, DC, 1993.
[13] T.J. Poinsot, S.K. Lele, Boundary conditions for direct simulations of compressible viscous flows, J. Comput. Phys. 101 (1992) 104–129.
[14] J. Patterson, J. Imberger, Unsteady natural convection in a rectangular cavity, J. Fluid Mech. 100 (1980) 65–86.